Journal of Tribology Science and Technology
Original Research Article
Publication Date: 30 September 2024
Submission Date: 10 June 2024
DOI: 10.70973/JTST.1.1.2024.26-37

EFFECT OF METALLURGICAL COMPATIBILITY ON TRIBOLOGICAL BEHAVIOUR IN DRY SLIDING CONTACT USING MOLECULAR DYNAMICS APPROACH

Sudhanshu Kumar[1*], Surajit Kumar Paul[1], Mayank Tiwari[1]
[1]Department of Mechanical Engineering, Indian Institute of Technology, Patna, 801103, India
[*]Corresponding author: sudhraj121@gmail.com

ABSTRACT

To thoroughly comprehend friction mechanism, especially those pertinent to nano-electromechanical and micro-electromechanical systems, it is essential to study surface interactions at the nanoscale. Sliding friction resulting from ploughing and adhesive wear that significantly impacts the performance of sliding components, used in NEMS/MEMS. The current work focuses on modelling of dry sliding contact between two hemispherical asperities, considering four material combinations: identical (Cu-Cu, Fe-Fe), partially metallurgically compatible (Fe-Cu), and metallurgically incompatible (Ni-Ag) using molecular dynamics (MD) simulations. At specific sliding speed, plastic deformation and atomic wear are observed in the study. Particularly high atomic wear is observed in the Cu-Cu tribopair due to the ease of slip within the FCC (face-centered cubic) crystal of copper. More dislocation activity is also induced in Cu-Cu combination as compared to Fe-Fe combination. Higher average friction coefficients are obtained for identical combinations compared to other material combinations. On the other hand, lower average friction coefficients and atomic wear are observed for metallurgically incompatible combinations compared to partially metallurgically compatible pairs. Understanding these interactions at the nanoscale is crucial for optimizing the performance and durability of small-scale components subject to sliding friction.

KEYWORDS: Dry sliding, molecular dynamics approach, friction coefficient, dislocation activity, wear volume, different metallic combination.

INTRODUCTION

Tribological contacts are responsible for ~23% of global energy consumption [1]. Of this, 20% is dedicated to overcoming friction, and 3% is utilized for remanufacturing worn parts and spare equipment due to wear and related failures [1]. To prevent tribological failure in the sliding components of NEMS devices, it is crucial to compute and optimize their friction and wear properties. Nanogears, nanowires, and nanotubes are critical components in NEMS devices, playing key roles in power transmission and signal transmission systems [2]. The functioning of these nanodevices in electric and mechanical systems is often crucial due to their high re-modelling costs. [3]. These devices can fail because of the frequent sliding of surfaces composed of different metals under critical conditions like contact pressure, lubrication, and spacing [4,5]. As surfaces slide against each other frequently, the rubbing action at the nanoscale leads to considerable adhesion force [6]. The adhesion force encompasses various forces, including van der Waals force, hydrogen bonding, electrostatic attraction, and ionic bonding, arising from the physical and chemical properties of contacting surfaces [7]. Recently, the molecular dynamics (MD) approach has been employed to simulate nano-deformation and scratching procedures [8–12].

The friction between sliding surfaces is determined by the interaction of asperities and the characteristics of the surface topography [13,14]. Copper (Cu), silver (Ag), and iron (Fe) possess superior thermal conductivity and provide suitable adhesive force during sliding action. Cu and Fe are widely used

in fabricating NEMS/MEMS devices through the chemical vapor deposition method [15]. Lin et al. [16] developed an MD model to study sliding contact on flat surfaces of a Cu-Fe tribopair, determining the friction coefficient and heat generation at the interface. There have also been attempts to simulate the contact between a hemispherical and a flat asperity [17–19]. Rabinowicz [20,21] investigated wear and friction coefficient between different material combinations using Pin-on disc set-up. Material compatibility and lubrication play a significant role in tribological action of sliding components. In the current research work, wear and friction coefficient are explored between hemispherical asperities of different material combinations using MD simulations.

Based on the literature outlined, it is evident that there have been limited but successful attempts in the past to explore the asperity wear, dislocation growth, and interacting mechanisms during the dry sliding motion of 3D hemispherical asperities [11,16,17,22,23]. In the present research work, 3D (three-dimensional) hemispherical asperities are constructed and sliding contact is simulated by performing the MD approach. Four tribopair (Cu-Cu, Fe-Fe, Fe-Cu and Ni-Ag) are considered, and friction and wear are evaluated under dry sliding motion.

1. SIMULATION METHODOLOGY

1.1 Depiction of a nanoscale contact

Fig. 1a shows the sliding contact between nanosurfaces used in NEMS/MEMS devices. These surfaces area actually rough and consist of thousands of asperities and their roughness depend on different scales. Fig. 1b shows schematic of two hemispherical asperities on the sliding surface. The hemispherical asperity of radius 70 Å is modelled on each surface. Respective atoms (e.g. Cu, Fe, Ni and Ag) are allocated in the upper and lower hemispherical asperities to make desired tribological combinations. The asperities are divided into two parts: the fixed layer and the movable layer, as illustrated in Fig. 1b. The depth of the fixed layer is 7 Å, and the rest is a movable or Newtonian layer. On a stiff foundation with a width of 7 Å, a stationary hemisphere asperity of the radius (*R*) 70 Å is constructed. Moreover, a movable hemispherical asperity with a radius of 70 Å and a base width of 7 Å is constructed. In Fig. 1b, interference (Δ) is basically termed as the distance measured perpendicularly between the apex of the hemispheres. The radius of asperity (R) is then used to non-dimensionalise the interference (Δ) such that further tribological analysis is easy to calculate. Hence, *Δ/R* is normalised interference.

Fig. 2a represents metallurgical compatibility chart between the selected combinations of metals and Fig. 2b shows schematic of reaction forces in sliding contact between two hemi-spherical asperities. The deformation and wear of Newtonian layer is observed here to correlate tribological characteristics for different combination of components. The normal and tangential forces are computed on the base of lower hemisphere atoms. The developed forces between the base and the Newtonian layer are calculated using a procedure developed by Bogusz et al. [24]. Only the sliding distance that keeps the asperities in contact is averaged to get these forces. The average friction coefficient is then computed using the formulas provided in Eqs 1-3.

$$F_{T,avg} = \frac{\sum_{n=n_i}^{n=n_0} F_{Tn}}{N} \quad (1)$$

$$F_{N,avg} = \frac{\sum_{n=n_i}^{n=n_0} F_{Nn}}{N} \quad (2)$$

$$\mu_{avg} = \frac{F_{T,avg}}{F_{N,avg}} \quad (3)$$

where, F_{Tn}, F_{Nn} are the friction force and normal force. The total timesteps from the beginning of contact to the asperities' separation is represented by the number N .

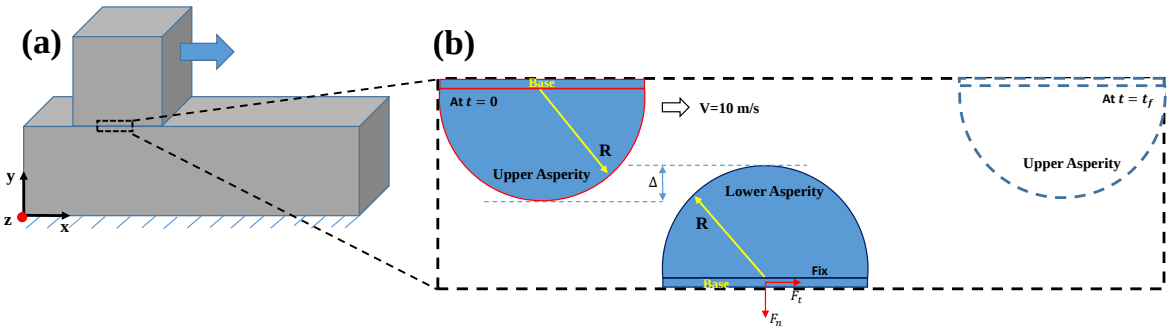

Fig. 1. (a) Schematic of a sliding contact between nanosurfaces used in NEMS/MEMS devices (b) Representation of sliding between two nano-asperities.

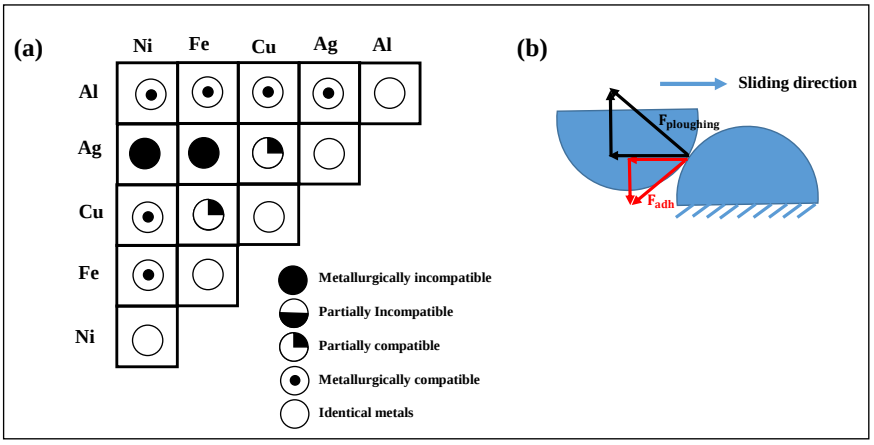

Fig. 2. (a) Metallurgically compatibility chart (b) Schematic of reaction forces in sliding contact between two hemi-spherical asperities.

1.2 Interaction potential considered in the modelling

A lot of work has gone into creating the metallic interaction simulation using the embedded atom method (EAM) [25–27]. Variations in electron density at the material's surface and bulk are taken into account by the EAM potential. [6,28]. Hence, for calculating the adhesive force between interacting surfaces, the EAM potential is more appropriate than the other potentials (e.g.: LJ etc.). Surface interactions and material wear at the interface may be significantly influenced by the electron density. In the current research work, atomic contacts between Cu-Cu, Fe-Cu and Fe-Fe are defined using the EAM potential established by Bonny et al. [29]. For Ni-Ag interaction, the EAM potential of Pan et al. [30] is applied here. The atomic system's total energy can be expressed as follows in Eq. 4 of EAM potential:

$$E_{total} = \sum_{i=1}^{N} \varepsilon_i \left[\sum_{j \neq i}^{N} D_j(r_{ij}) \right] + \frac{1}{2} \sum_{i,j \neq i}^{N} \phi_{ij}(r_{ij}) \qquad (4)$$

where, ε_i is the amount of energy required to embed i^{th} atom into electron density D_j produced by surrounded particles of i^{th} atom. ϕ_{ij} is the electrostatic potential among particles of r_{ij} separation distance.

1.3 Simulation technique

Initially, the system's total potential energy is computed using Eq. 4, and forces are determined by differentiating this potential energy with the position of atoms. Subsequently, the system is stabilized at a temperature of 300 K for 14 ps to allow particles to settle into equilibrium positions by minimizing energy. The differential equations of motion are integrated using the Velocity-Verlet technique [35] at a timestep of 0.002 ps, which enables the trajectory to be recorded of each atom. All calculations regarding the position/velocity of atoms are conducted within the NVE ensemble, ensuring the constancy of the number of atoms, energy, and volume throughout the simulation integration.

LAMMPS software is used to do MD simulations for time of 4370 ps [35]. Following this, the base of the upper hemisphere is imparted with a velocity of 0.1 Å/ps in the +x-direction, while the lower hemisphere rests static. The interactions among atoms may cause displacements due to generated reaction force. The "Open Visualisation Tool" (OVITO) is used to visualise and analyse each simulation's findings [36]. The "Dislocation Extraction Algorithm" (DXA) [38,39] is used to analyse dislocations and their associated vectors [37], and the local lattice arrangement of atomic structures is characterized using "Common Neighbor Analysis" (CNA) [40,41].

Non-periodic boundary condition is applied along the y-direction, and periodic boundary conditions are applied in the x- and z-axes. At each timestep, generated forces on atoms of the base are noted and added to determine forces on the lower hemisphere, from which the friction force (F_{Tn}) and normal force (F_{Nn}) are derived. To assess wear in the lower asperity, various cut-off distances are considered, once potential energy crosses this crucial threshold and becomes zero. For copper asperity, 5.5 Å is the chosen cut-off distance [29], however, because of the stronger metallic link in the iron element, a somewhat greater cut-off distance of 6.2 Å is used for iron asperity [31]. For silver (Ag) asperity, a cut-off distance of 5.9 Å is utilized [42]. The spherical form of critically displaced atoms is taken into consideration in order to calculate the wear volume, and the lower hemispherical asperity's wear volume is divided by the sliding distance to determine the wear rate (V_w) . Table 1 provides the input parameters needed to run the MD simulation.

Table 1: A list of the parameters for input

Parameters	Different material interactions			
	Ni-Ag	Fe-Cu	Cu-Cu	Fe-Fe
Radius, *R* (Å)	70	70	70	70
Atom count on the higher asperity	90956	84691	84869	84688
Atom count on the lower asperity	60663	85904	85904	86911
Normalized Interference, *Δ/R*	0.1	0.1	0.1	0.1
Time increment step (ps)	0.002	0.002	0.002	0.002
Starting temperature (K)	300	300	300	300
Stabilization time (ps)	14	14	14	14
Total time (ps)	4370	4370	4370	4370

2. RESULTS AND DISCUSSION

2.1 Deformation in asperities

The sliding process undergoes two distinct phases: the first half sliding, where contact initiates between asperities until their centers align vertically, and the subsequent second half sliding. In the case of Fe-Cu interaction depicted in Figure 3a, contact initiation occurs at 1200 ps, signaling the onset of ploughing action. By the time of 1310 ps, the copper asperity atoms are ploughed out when the upper asperity progresses, evident from the demarcated region in Figure 3b, with ploughing predominantly occurring during the first half sliding. Subsequently, as the sliding process continues, fewer atoms stand in the way as obstacles. Alignment of the hemispheres vertically is reached by 1740 ps, as shown in Figure 3c, observing a considerable amount of attached atoms on the upper asperity by 3115 ps, depicted in the demarcated region of Figure 3d. In order to extract these attached atoms from the lower asperity, the adhesion force subsequently generates a response force.

Consequently, the ploughing force dominates until the centers of both asperities align vertically. In the latter half sliding, adhesion force becomes predominant in establishing friction between surfaces until both asperities detached, as reported by earlier researchers [6] in a metallic interaction (Cu-Cu). When the asperities are fully out of contact (see in Figure 3e), no neck

development is observed at 3115 ps. The final position of deformed asperities post-simulation completion at 4370 ps is illustrated in Figure 3f, while Figure 3g provides a three-dimensional perspective view of the interaction, highlighting the consideration of three-dimensional sliding contact in this study.

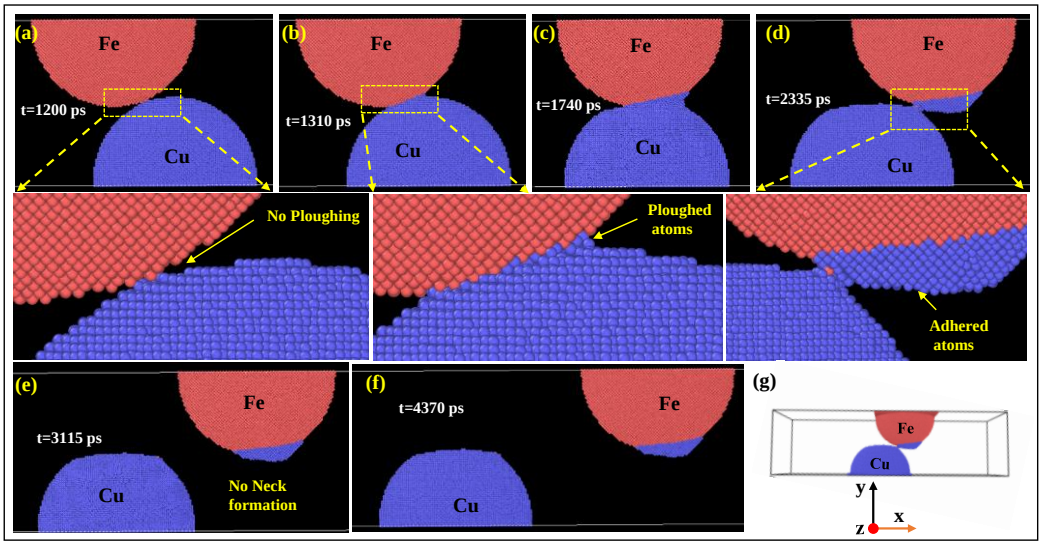

Fig. 3: Lower asperity deformation with time as the top asperity slides at a normalised interference of 0.1. (a) Just before asperities come into touch, (b) Atoms begin to plough at 1310 ps, (c) At the moment of 1740 ps, when asperities align vertically, (d) Asperity deformation at 2335 ps, (e) and (f) are front views of interacting asperities at respective times, (g) is three-dimensional perspective view.

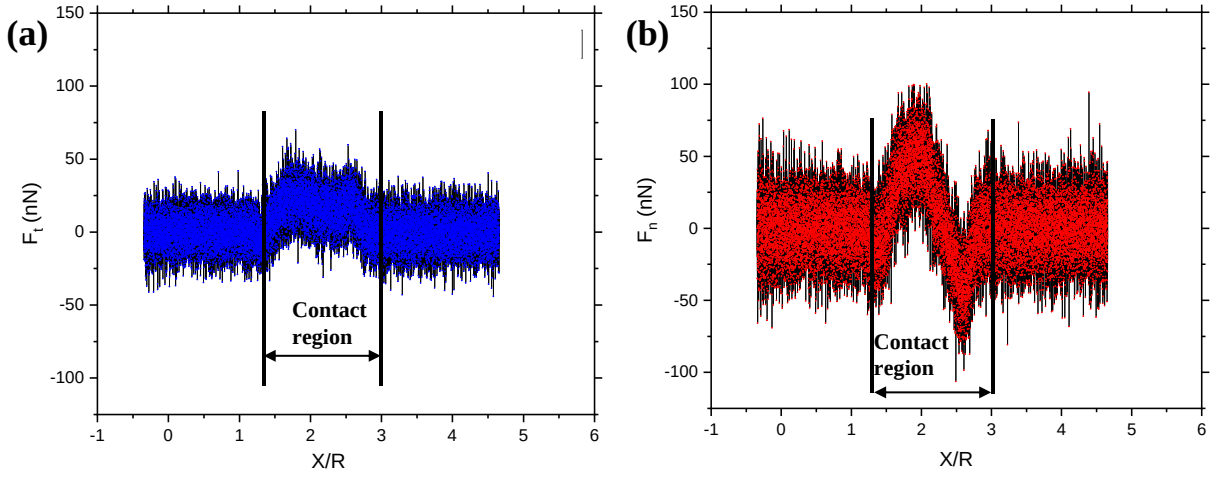

Fig.4: Variation of Traction Force and Normal force on lower asperity for Fe/Cu interaction (a) Traction force at interference (Δ/R) of 0.1, (b) Normal force at interference (Δ/R) of 0.1.

For the case of Fe/Cu material interaction, the total traction and normal reaction forces are computed and plotted with respect to normalised sliding distance (X/R) in Fig. 4. As the upper asperity starts to slide on lower fixed asperity, deformation starts and sticking of atoms occur. The ploughing force is acting here due to deformation of asperities whereas adhesive force acts here because of sticking of atoms. As traction force is sum of tangential components of ploughing force and adhesion force, it starts increasing from zero and approaches to maximum when X/R=1.6. This is just before the alignment of asperities at X/R=2. After that, traction force starts decreasing and becomes zero at the end of contact because ploughing force got decreasing as lot of deformation has already occurred. Similarly, normal force is the normal components of ploughing

and adhesion force. As the upper asperities approaches towards lower asperity, normal force also increases and becomes maximum approximately at X/R=2 when asperities align to each other. The alignment of asperities means the centre of both asperities are aligned vertically. Similarly, maximum normal reaction force is found at the same sliding distance (at X/R where asperities align vertically) by researchers using finite element method for hard (Fe) and soft (Al) material interaction [31,32]. And then normal force changes direction because of strong adhesive force and lower ploughing force. Similar, trend of traction and normal forces with respect to sliding distance is also found in literatures for soft-to-soft material (Cu/Cu) interaction [33].

2.2 The effect of material compatibility on friction

Fig. 5 shows the sliding interaction of Ni-Ag metals and Fe-Fe metals at normalised interference (Δ/R) of 0.1 for different sliding time. Fig. 6 represents the variation of average friction and normal force at normalised interference (Δ/R) of 0.1 for the different metallic pair. These reaction force consists of ploughing and adhesion forces coming out while sliding action.

The average friction force and normal force for Ni-Ag pair are relatively lesser than other metallic pairs. Moreover, Average friction coefficient is also lesser than the rest of other pairs. An increase in material compatibility is seen to enhance both normal and friction force. Chen et al. [34] also observed a comparable range of average friction coefficient (0.11-1.50) by using pin-on-disc tribometer with vacuum and dry circumstances for extremely pure grades of iron and copper metals. Jellison [35] performed a vacuum-controlled pin-on-disc sliding test between Cu alloys and discovered an average friction coefficient that was nearly equal to 2, comparable to that of the current model of Cu-Cu contact. Adhesion is responsible for frictional contact in the interaction of these materials in a vacuum of space. The sliding tests are also performed between 1020 steel and copper alloy in a vacuum by Jellison et al. and found the friction coefficient near about 1.

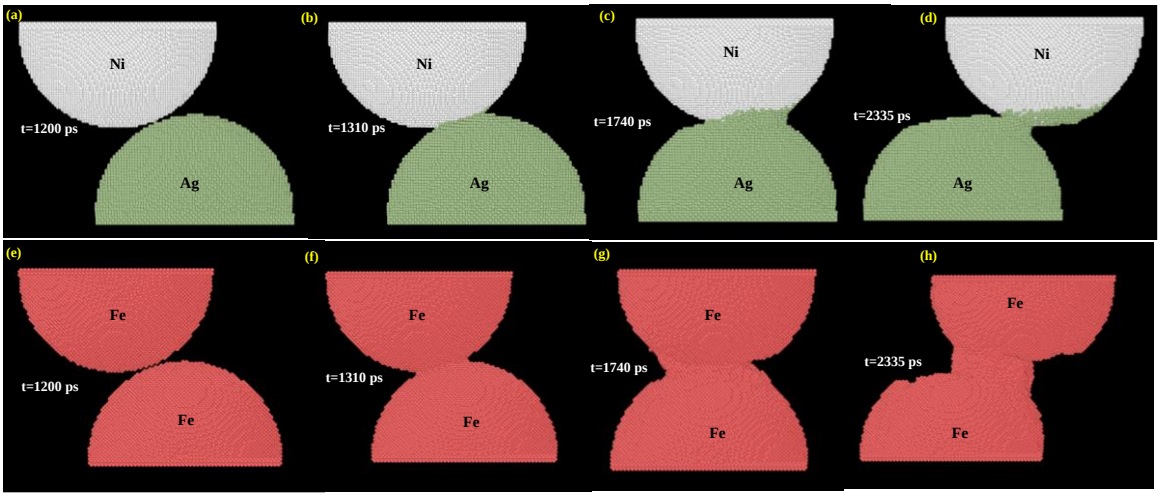

Fig. 5. Lower asperity deformation with time as the top asperity slides at a normalised interference of 0.1 in Ni-Ag and Fe-Fe metallic combination. (a) Just before asperities come into touch, (b) Atoms begin to plough at 1310 ps, (c) At the moment of 1740 ps, when asperities align vertically, (d) Asperity deformation at 2335 ps for Ni-Ag metallic combination; (e) (f), (g) and (h) are at respective times for Fe-Fe metallic combination.

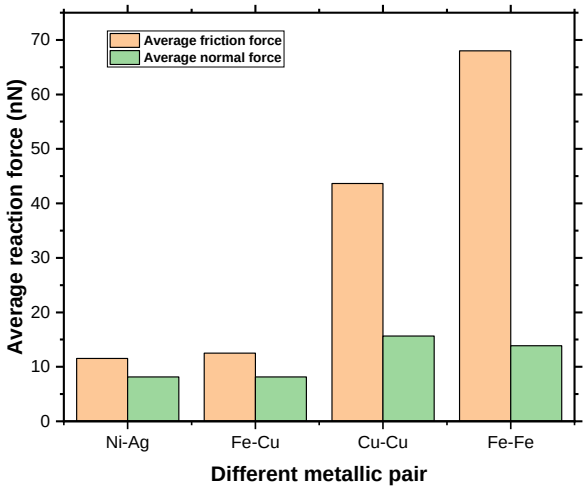

Fig. 6. Average friction and normal force for different metallic pair.

Table 2: Average coefficient of friction for dissimilar metallic pair at normalised interference of 0.1

Metallic pairs	Ni-Ag	Fe-Cu	Cu-Cu	Fe-Fe
Average friction coefficient (μ_{avg})	1.416	1.526	2.793	4.904

Rabinowicz [36,37] conducted sliding tests on many materials and found a high coefficient of friction and adhesive wear coefficient in sliding contact of identical types of materials. Identical metals have the tendency to get fully miscible in the solid state. It is due to the higher metallurgical compatibility of these metals. Compatibility refers to the degree of atomic attraction of contacting metals [37]. It may be due to higher metallic bonding between the same type of metals. As metallic bond strength depends on unpaired or free electrons in the valence shell of metals [38]. The unpaired electrons are more in the iron metal than that in Copper, so higher metallic bond strength is induced in iron compared to Copper. Higher metallic bond strength gives higher adhesive force since it is a component of adhesive force [7]. The ploughing force is also high because the deformation of Fe is quite difficult relative to Cu. Consequently, a higher friction force is obtained for Fe-Fe compared to Ni-Ag, Fe-Cu and Cu-Cu interactions for the interference of 0.1, as found in Fig. 6.

Nucleation of dislocations has been found to be a prerequisite for changes in both normal force and friction force [39]. Wear, plastic deformation and strain-hardening could all be caused by these dislocations. Bowden et al. [40] also provided the idea about excessive wear and higher friction force due to identical physical properties of interacting materials. Rabinowicz conducted static friction experimental tests and found a static friction coefficient between pairs of twenty metals. Static friction coefficient directly depends on the surface interfacial energy of adhesion [20]. And the surface interfacial energy of adhesion is the function of metallurgical compatibility of interacting surfaces that becomes more for higher compatible materials [20]. Generally, the sliding friction coefficient also depends on the compatibility of interacting surfaces [37]. As friction force opposes relative motion between moving pairs, the energy given to the components of NEMS/MEMS devices is consumed by friction force; as a result, the efficiency of the device reduces. The clever materials selections from the Rabinowicz chart based on metallurgical compatibility and desired physical properties (thermal conductivity, melting point, electrical conductivity, etc.) are needed by the designer to make the smooth operation of devices to reduce frictional losses and wear.

2.3 Effect of material compatibility on atomic wear

Figs. 7a-7f shows deformation of copper asperity as sliding proceeds for normalised interference of 0.1. Fig. 7a illustrates that the motion of upper asperity begins in identical material contact (Cu-Cu). Atoms are going to plough on both asperities when they collide at 1700 ps of sliding time (see Fig. 7a). A sliding time of 1740 ps is reached when both asperity's atoms are ploughed (Fig. 7b). After time of 1740 ps, the ploughed atoms of each asperity adhered due to identical material interactions. The asperities got vertically aligned at the time of 2300 ps in Fig. 7c. As can be seen in the demarcated region of Figure 7d, the ploughed atoms of upper asperity are found to have been moved to lower asperity. From lower asperity to upper asperity, atoms likewise undergo comparable changes. Adhered atoms do not separate readily when Asperities are still sliding and begin to break away from contact, as Fig. 7e illustrates. At sliding time (t) = 3690 ps, a neck is detected and furthermore, as seen in Fig. 7f, the neck elongates along the advantageous slip plane until breaking at sliding time (t) = 4370 ps.

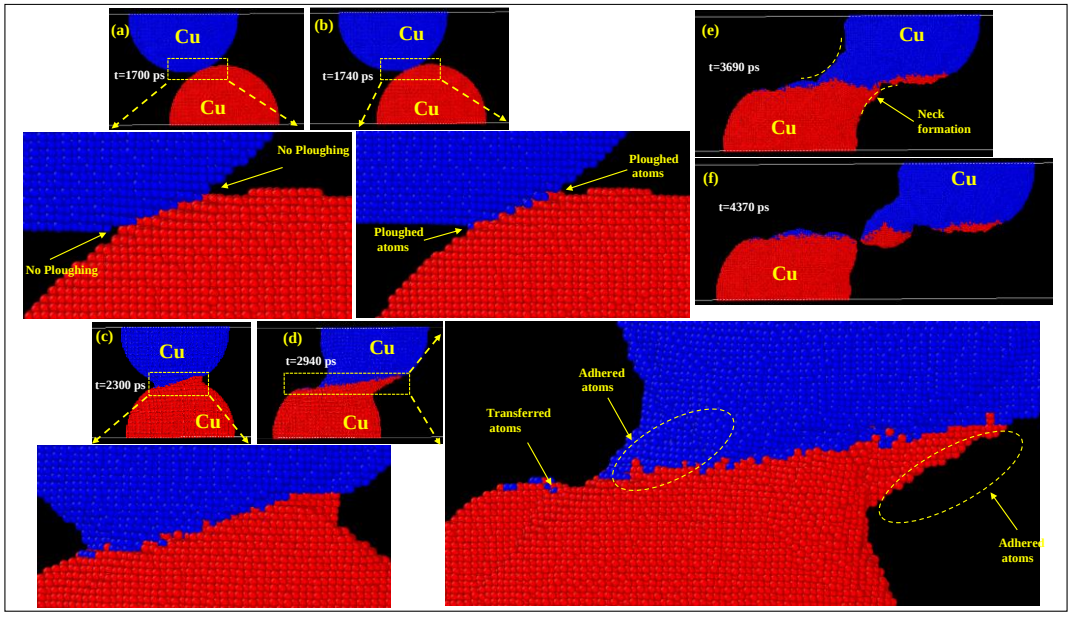

Fig. 7: Deformation in copper asperities (a) at time (t) = 1700ps (b) at time (t) = 1740 ps (c) at time (t) = 2300 ps (d) at time (t) = 2940 ps (e) at time (t) = 3690 ps (f) at time (t) = 4370 ps.

The wear rate (V_w) is defined as the wear volume for unit sliding distance in accordance with Archard's wear law. In a similar way, wear rate computation using the MD technique has been documented previously [41]. The wear rate variation for several material combinations at normalised interference (Δ/R) of 0.1 is depicted in Fig. 8. Comparing the wear rate for partial compatibility of materials (Fe-Cu) and incompatible materials (Ni-Ag), it has been noted that for identical material interactions (Fe-Fe and Cu-Cu), the atomic wear rate is greater. However, because of the more deformation in asperity, the Cu-Cu combination exhibits the largest wear rate. However, maximum wear rate is observed for Cu-Cu combination due to high deformation of asperities. In previous literature, an identical metallic interaction also showed a higher wear rate [37,42,43]. Strong adhesion forces are created when atoms of identical materials meet, causing some atoms to stick to one another until the sliding process is finished.

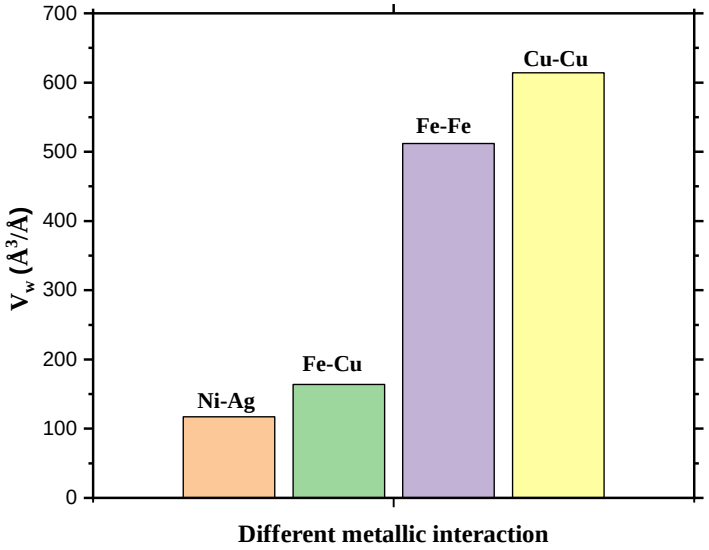

Fig. 8. Atomic wear rate for various interactions of metals at normalised interference (Δ/R) of 0.1.

Dislocation analysis is necessary to understand the plastic deformation in the Cu-Cu asperity interaction. Partial dislocations such as Shockley(1/6<112>), Stair-rod(1/6<110>) and Hirth(1/3<001>) are generated in both asperities at 2335 ps in the Fig. 9a. As the sliding motion proceeds, perfect dislocation (1/2<110>) generates at the time of 3200 ps in the Fig. 9b. Similarly, Frank dislocation (1/3<111>) also appears at this time, and other dislocations also become prolonged, as found in the Fig. 9b. Stair-rod, Frank and Hirth dislocations are immovable and causes of strain hardening in the material. These defects are also called sessile dislocation, which creates jamming of movable dislocations and is responsible for generating back stress in the asperity. Shockley partial dislocation is movable in their slip plane, which is responsible for plastic deformation occurring in the asperities.

An Fe- Fe interaction is also simulated at an interference of 0.1. Once the sliding of asperities starts, plastic deformation in the form of dislocations is generated. The perfect screw dislocation (1/2<111>) is generated in both asperities at a time of 2335 ps as found in Fig. 9c. The sessile edge dislocations (<100>) are also generated in both asperities at a time of 2335 ps. As the sliding continues, dislocation of type <110> also originates at a time of 3200 ps in Fig. 9d. As this material interaction is also of identical type, necking is formed before the end of the contact, which is shown in Fig. 9d.

The adhesive wear coefficient is higher for identical types of dry metallic interaction [37], which makes more wear in identical types of metallic interaction according to Archard wear theory [37,42,43]. As a result, atomic wear is higher in Fig. 8 for the identical types of material interaction compared to partial compatibility or incompatibility of materials. When identical types of metals interact, then a strong adhesion force sticks to the interacting atoms. Until the entire sliding process is finished, some atoms stay stuck to one another, and a neck is constructed and elongated while the sliding proceeds. The lattice structure of Fe is body centered cubic (BCC) means; less ductile at the macro-level, whereas the lattice structure of Cu is face centered cubic (FCC). The slip systems are lesser in BCC than that in FCC. Therefore, the slipping of atoms is easier in FCC crystal of Copper metal. Due to the sliding action; atoms slip easily in the FCC crystal structure of copper asperity in Cu-Cu interaction and make a dense forest of dislocations at 3200 ps as found in the Fig. 9b. As Fe element also has more metallic bond strength than Cu element [38]. This is also why the Cu-Cu interaction has a denser population of dislocations than the Fe-Fe interaction. So, relatively lesser atomic displacement or wear is found in the Fe-Fe combination than in the Cu-Cu combination, according to the bar chart shown in Fig. 8.

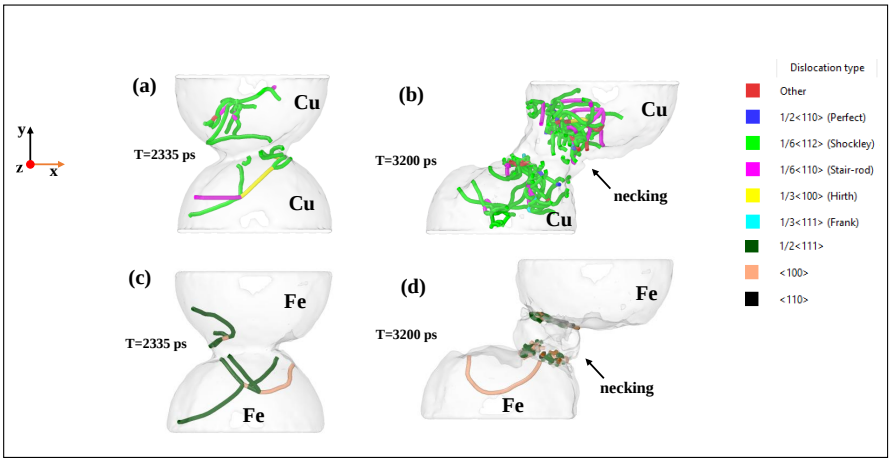

Fig. 9: Appearance of dislocation in the sliding for the interference of 0.1, (a) and (b) for interaction of Cu –Cu, (c) and (d) for interaction of Fe-Fe.

CONCLUSIONS

In the current research work, the friction and wear for various metals combinations under dry sliding conditions are calculated using molecular dynamics (MD) approach. Key conclusions drawn from this work are as follows:

(1) Ultimately, the wear rate is determined by how well interacting tribo-surfaces are metallurgically compatible. Incompatible materials have a reduced wear rate. Only with similar material interactions, necking is observable, and this behaviour results in a higher wear rate.

(2) Average friction coefficient is calculated for various combinations of materials. It is discovered that the friction coefficient rises for the combinations of Ni-Ag, Fe-Cu, Cu-Cu, and Fe-Fe, in that sequence.

(3) As the sliding continues, partial dislocations are seen to transition into perfect dislocations.

REFERENCES

[1] Holmberg K, Erdemir A. Influence of tribology on global energy consumption, costs and emissions. Friction 2017;5:263–84. doi:10.1007/s40544-017-0183-5.

[2] Berman D, Krim J. Surface science, MEMS and NEMS: Progress and opportunities for surface science research performed on, or by, microdevices. Prog Surf Sci 2013;88:171–211. doi:10.1016/j.progsurf.2013.03.001.

[3] Tariq Jan M, Hisham Bin Hamid N, Md Khir MH, Ashraf K, Shoaib M. Reliability and fatigue analysis in cantilever-based MEMS devices operating in harsh environments. J Qual Reliab Eng 2014;2014. doi:10.1155/2014/987847.

[4] Kumar S, Rajput A, Paul SK. Friction and wear study of metallic contacts under dry sliding conditions : A molecular dynamics simulation-based approach. J Eng Tribol 2023. doi:10.1177/13506501231220076.

[5] Kumar S, Rajput A, Kumar Paul S, Tiwari M. Molecular dynamics simulation of dry sliding between non-Gaussian copper rough surfaces. Appl Surf Sci 2024;664:160220. doi:10.1016/j.apsusc.2024.160220.

[6] Vadgama BN. Molecular Dynamics Simulations of Dry Sliding Asperities to Study Friction and Frictional Energy Dissipation. Auburn University, 2014.

[7] Bhushan B. Introduction to Tribolgy. Second. Ohio: John Wiley & Sons; 2013.

[8] Zhang J, Zhang J, Wang Z, Hartmaier A, Yan Y, Sun T. Interaction between phase transformations and dislocations at incipient plasticity of monocrystalline silicon under nanoindentation. Comput Mater Sci 2017;131:55–61. doi:10.1016/j.commatsci.2017.01.043.

[9] Shi J, Shi Y, Liu CR. Evaluation of a three-dimensional single-point turning at atomistic level by a molecular dynamic simulation. Int J Adv Manuf Technol 2011:161–71. doi:10.1007/s00170-010-2929-3.

[10] Fang T, Weng C. Three-dimensional molecular dynamics analysis of processing. Nanotechnology 2000;11:148–53.

[11] Hu PZY. Molecular Dynamics Study on Friction Due

to Ploughing and Adhesion in Nanometric Scratching Process. Tribol Lett 2011:41–6. doi:10.1007/s11249-010-9681-6.

[12] Zhang Z, Alabd I, Herbert A. Scratching an Al / Si Interface : Molecular Dynamics Study of a Composite Material. Tribol Lett 2018;66:1–12. doi:10.1007/s11249-018-1038-6.

[13] Jackson RL, Green I. A statistical model of elasto-plastic asperity contact between rough surfaces. Tribol Int 2006;39:906–14. doi:10.1016/j.triboint.2005.09.001.

[14] Kumar S, Paul SK, Tiwari M. Assessment of surface and subsurface evolution under rolling contact fatigue of a pearlitic steel. Mater Today Commun 2023;35:105803. doi:10.1016/j.mtcomm.2023.105803.

[15] Professor William N. Sharpe J, editor. Springer Handbook of Experimental Solid Mechanics. Baltimore: 2008.

[16] Lin E, Niu L, Shi H, Duan Z. Applied Surface Science Molecular dynamics simulation of nano-scale interfacial friction characteristic for different tribopair systems. Appl Surf Sci 2022;258:2022–8. doi:10.1016/j.apsusc.2011.04.117.

[17] Cha P, Srolovitz DJ, Vanderlick TK. Molecular dynamics simulation of single asperity contact. Acta Mater 2004;52:3983–96. doi:10.1016/j.actamat.2004.05.014.

[18] Landman U, Luedtke WD, Gao J. Atomic-Scale Issues in Tribology : Interfacial Junctions. Langmuir 1996;I:4514–28.

[19] Song J, Srolovitz DJ. Atomistic simulation of multicycle asperity contact. Acta Mater 2007;55:4759–68. doi:10.1016/j.actamat.2007.04.042.

[20] Taylor P, Rabinowicz E. The Determination of the Compatibility of Metals through Static Friction Tests The Determination of t h e Compatibility o f Metals t h r o u g h Static Friction Tests. Tribol Trans 2008:37–41.

[21] Rabinowicz E. - 541 533 the least wear. Wear 1984;100:533–41.

[22] Zhong J, Adams JB, Hector LG. Molecular dynamics simulations of asperity shear in aluminum. J Appl Phys 2020;4306. doi:10.1063/1.1558966.

[23] Karthikeyan S, Agrawal A, Rigney DA. Molecular dynamics simulations of sliding in an Fe – Cu tribopair system. Wear 2009;267:1166–76. doi:10.1016/j.wear.2009.01.032.

[24] Bogusz S, Cheatham TE, Brooks BR, Bogusz S, Iii EC, Brooks BR. Removal of pressure and free energy artifacts in charged periodic systems via net charge corrections to the Ewald potential Removal of pressure and free energy artifacts in charged periodic systems via net charge corrections to the Ewald potential. J Chem Phys 1998;7070. doi:10.1063/1.476320.

[25] Mishin Y. Structural stability and lattice defects in copper : Ab initio , tight-binding , and embedded-atom calculations. Phys Rev B 2001;63:1–16. doi:10.1103/PhysRevB.63.224106.

[26] Mendelev MI, Han S, Srolovitz DJ, Ackland GJ, Sun DY, Asta M, et al. Development of new interatomic potentials appropriate for crystalline and liquid iron. Philos Mag 2010;6435. doi:10.1080/14786430310001613264.

[27] Starikov S V, Smirnova DE. Angular-dependent interatomic potential for large-scale atomistic simulation of iron : Development and comprehensive comparison with existing interatomic models. Phys Rev Mater 2021. doi:10.1103/PhysRevMaterials.5.063607.

[28] Plimpton SJ, Hendrickson BA. PARALLEL MOLECULAR DYNAMICS WITH THE EMBEDDED ATOM METHOD STEVEN J. PLIMPTON and BRUCE A. HENDRICKSON Sandia National Laboratories, Albuquerque, NM 87185. MRS Proc 1993.

[29] Bonny G, Pasianot RC, Castin N, Malerba L, Pasianot RC, Castin N, et al. Ternary Fe – Cu – Ni many-body potential to model reactor pressure vessel steels : First validation by simulated thermal annealing. Philos Mag 2009;6435. doi:10.1080/14786430903299824.

[30] Pan Z, Borovikov V, Mendelev MI, Sansoz F. Development of a semi-empirical potential for simulation of Ni solute segregation into grain boundaries in Ag. Model Simul Mater Sci Eng 2018;26. doi:10.1088/1361-651X/aadea3.

[31] Jackson RL, Duvvuru RS, Meghani H, Mahajan M. An analysis of elasto-plastic sliding spherical asperity interaction. Wear 2007;262:210–9. doi:10.1016/j.wear.2006.05.011.

[32] Faulkner A, Arnell RD. The development of a finite element model to simulate the sliding interaction between two , three-dimensional , elastoplastic , hemispherical asperities. Wear 2000:114–22.

[33] Harris DK. Molecular scale analysis of dry sliding copper asperities. Appl Nanosci 2015:469–80. doi:10.1007/s13204-014-0339-9.

[34] Chen LI, Rigney DA. TRANSFER DURING UNLUBRICATED SLIDING WEAR OF SELECTED METAL SYSTEMS*. Wear 1985;105:47–61.

[35] Taylor P, Jellison J, Predmore R, Staugaitis CL. Sliding Friction of Copper Alloys in Vacuum 2008:37–41. doi:10.1080/05698196908972259.

[36] Rabinowicz E. Friction and Wear of Materials. Second. John Wiley & Sons; 1995.

[37] Rabinowicz E. Magnitude , Scatter , Uses © O. J Lubr Technol 2017;103.

[38] Gardel M, Schwarz U, Hoore M, Rack K. The mechanism of the metallic adhesion bond. J Phys D

1972.
[39] Li B, Li J, Zhu P, Xu J, Li R, Yu J. Applied Surface Science In fl uence of crystal anisotropy on deformation behaviors in nanoscratching of AlN. Appl Surf Sci 2019;487:1068–76. doi:10.1016/j.apsusc.2019.05.218.
[40] Bowden F P. The nature of sliding and the analysis of friction 1938.
[41] Yang Y, Huang L, Shi Y. Adhesion suppresses atomic wear in single-asperity sliding. Wear 2016;352–353:31–41. doi:10.1016/j.wear.2016.02.002.
[42] Rabinowicz E. An adhesive wear model based on variations strength values in. Wear 1980;63:175–81.
[43] Archard JF. Contact and Rubbing of Flat Surfaces. J Appl Phys 1953;981. doi:10.1063/1.1721448.

